

---

# A Physics-Inspired Optimizer: Velocity Regularized Adam

---

Pranav Vaidhyanathan<sup>1,3\*</sup> Lucas Schorling<sup>1,5\*</sup> Natalia Ares<sup>1,5</sup> Michael A. Osborne<sup>1,3†</sup>

<sup>1</sup> University of Oxford, United Kingdom

<sup>3</sup>{pranav, mosb}@robots.ox.ac.uk

<sup>5</sup>{lucas.schorling, natalia.ares}@eng.ox.ac.uk

## Abstract

We introduce Velocity-Regularized Adam (VRAdam), a physics-inspired optimizer for training deep neural networks that draws on ideas from quartic terms for kinetic energy with its stabilizing effects on various system dynamics. Previous algorithms, including the ubiquitous Adam, operate at the so called adaptive edge of stability regime during training leading to rapid oscillations and slowed convergence of loss. However, VRAdam adds a higher order penalty on the learning rate based on the velocity such that the algorithm automatically slows down whenever weight updates become large. In practice, we observe that the effective dynamic learning rate shrinks in high-velocity regimes, damping oscillations and allowing for a more aggressive base step size when necessary without divergence. By combining this velocity-based regularizer for global damping with Adam’s per-parameter scaling to create a hybrid optimizer, we demonstrate that VRAdam consistently exceeds the performance against standard optimizers including AdamW. We benchmark various tasks such as image classification, language modeling, image generation and generative modeling using diverse architectures and training methodologies including Convolutional Neural Networks (CNNs), Transformers, and GFlowNets.

## 1 Introduction

Optimizing the parameters of deep neural networks remains a cornerstone of progress in machine learning. Improving on the core idea of Stochastic Gradient Descent (SGD) Sutskever et al. [2013], adaptive methods like Adam (Adaptive Moment Estimation) Kingma and Ba [2017] have become ubiquitous due to their practical effectiveness across diverse tasks and architectures. Despite its success, the performance of Adam can be sensitive to hyperparameter choices and its training dynamics can exhibit instabilities Reddi et al. [2019]. Furthermore, fully understanding the training dynamics of deep neural networks remains an open challenge Wang and Choromanska [2025], and even small improvements to existing optimization algorithms can often lead to significant reductions in resource consumption.

One line of work, observed empirically, is that training often occurs at the edge of stability Cohen et al. [2022, 2024], a regime for which the largest eigenvalue, also called sharpness, of the loss Hessian equilibrates around a fixed value proportional to the inverse of the learning rate (LR). This seems in contrast with common presumptions in classical optimization theory and has profound implications for convergence speed, stability, and generalization. In classical optimization, higher LRs lead to faster convergence at the cost of oscillations or divergence if stability constraints (depending on the loss landscape) are violated Boyd and Vandenberghe [2004]. This pathological behaviour of optimizers, like AdamW, leads to instabilities and slowed convergence of the loss.

---

\*Equal Contribution

†Corresponding author

These challenges motivate the exploration of alternative optimization strategies. In line with the origins of machine learning itself Hopfield [1982], Ackley et al. [1985], one promising avenue draws inspiration from physics. For that, the optimization trajectory is conceptualized as a discretized motion of a particle within the high-dimensional loss landscape. Both from the structure of the “potential” landscape and the discretization, instabilities may arise from excessive “velocity” or overly large step sizes. This perspective suggests that mechanisms from high-energy and non-classical physics applied to optimization can improve aspects of stability. Building upon the established success of momentum, which incorporates velocity into gradient updates, recent ideas have explored a maximal velocity, drawing parallels to the speed of light in the theory of special relativity França et al. [2020].

This work introduces a class of physics-inspired optimizers, termed Velocity-Regularized Adam (VRAdam), designed to improve upon the stability and performance of standard adaptive methods Kingma and Ba [2017], Loshchilov and Hutter. Inspired by quartic terms used to model kinetic energy in more stable systems such as classical time crystals Shapere and Wilczek [2012] and heavy quark modeling using non-relativistic quantum chromodynamics (NRQCD) Braaten [1997] known for their unique stability properties, VRAdam introduces a novel regularization mechanism. This mechanism controls the effective learning rate  $\eta$  via penalizing high velocity, namely  $\eta_t = \alpha_0 / (1 + \min(\beta_3 ||v_t||^2, \alpha_1))$ . Crucially, this regularization can be configured to depend on either the norm of the optimizer’s velocity  $||v_t||$  (i.e., the momentum buffer) or the norm of the gradient itself.

Equipped with this new optimizer, VRAdam, we probe its dynamics at the adaptive edge of stability, observe faster convergence, and analyze its sharpness. With well-tuned hyperparameters, we benchmark VRAdam against AdamW, SGD with Nesterov momentum and RMSProp on image classification with the CIFAR-10 dataset and convolutional neural network architecture, on language modeling with transformers on the WikiText2 dataset and a generative modeling task with GFlowNets and report improved performance on all tasks by up to 63%. Furthermore, we report low hyperparameter sensitivity on a diffusion model trained on the handwritten digit dataset, MNIST.

With this work, we contribute:

- VRAdam, a physics-inspired and interpretable modification to AdamW,
- Adaptive edge of stability analysis of VRAdam with faster convergence,
- VRAdam outperforms AdamW and other optimizers on a wide range of benchmarks.

## 2 Background

**Edge of stability.** The training of deep neural networks does not follow classical optimization trajectories when trained with full-batch gradient descent (GD). However, during training, these models experience a surprising phase called the edge of stability (EoS). In this phase, the loss Hessian’s largest eigenvalue ( $\lambda_{\max}$ ) rises to approximately  $2/\eta$ , the numerical stability limit determined by the learning rate  $\eta$ . At EoS, the eigenvalue persists at this threshold, causing short-term, non-monotonic oscillations in the loss function. Despite these oscillations, the model still achieves long-term descent in the loss, though at the cost of slower convergence Arora et al. [2022], Cohen et al. [2022].

More recently, empirical bounds on the adaptive edge of stability (AEoS) have been observed for adaptive optimizers such as Adam Cohen et al. [2024]. Here, the relevant stability threshold involves preconditioning the Hessian  $H_t$ , where the precondition is constructed from the exponential moving average (EMA) of past element-wise squared gradients  $m_t$ :

$$P_t^{-1} H_t, \quad P_t = \text{diag}(\sqrt{m_t} + \varepsilon), \quad (1)$$

This adaptive preconditioning coincides with the learning rate scaling in Adam (see Alg. 1) and scales down the step size in high-variance (typically high-curvature) directions as well as scales up in low-variance ones. Since the local stability of an optimizer around a minimizer depends on the eigenvalues of the quadratic Taylor approximation  $L(x) \approx \frac{1}{2}x^\top H x$ , Adam’s dynamics are shown to be stable Cohen et al. [2024] as long as

$$\lambda_{\max}(P_t^{-1} H_t) < \frac{2 + 2\beta_1}{(1 - \beta_1)\eta} = \frac{38}{\eta} \quad (\beta_1 = 0.9). \quad (2)$$

However, as this threshold is attained, the adaptive oscillatory regime can slow final convergence, as the optimizer continually adjusts its preconditioner to maintain stability as well Song and Yun [2023].

**Physical origins of exotic Lagrangians.** To better comprehend and navigate the edge of stability regime, we can draw inspiration from the physics governing complex optimization scenarios. The deep insights provided by the interplay of physics and machine learning frameworks have been demonstrated in various scenarios, such as the improved interpretation of Neural Tangent Kernels (NTK) through Langevin dynamics Avidan et al. [2025]. One central concept in physics is the Lagrangian  $\mathcal{L}(x, v) = T(v) - V(x)$  of a system, which is a function of position  $x$  and velocity  $v$  and (typically) defined as the difference between kinetic energy  $T$  and potential energy  $V$  from which the equation of motion can be derived via the Euler-Lagrange equation. In this work, we investigate non-standard Lagrangian formulations of physical phenomena with excellent stability conditions. For example, the stability of seemingly disparate quantum systems like heavy quarkonia (described by NRQCD) and classical time crystals share conceptual parallels rooted in higher-order velocity terms. These terms fundamentally reshape energy landscapes by creating non-standard dispersion relations, establishing invariant submanifolds in phase space where stable configurations emerge as attractors or limit cycles. By explicitly breaking certain symmetries—Lorentz invariance in NRQCD and time-translation in time crystals—these higher-order kinetic terms paradoxically enhance stability through topological protection mechanisms and the generation of emergent length/time scales Niemi [2021], Guha and Ghose-Choudhury [2019].

As a demonstration of this phenomenon, we can consider Nonrelativistic QCD (NRQCD), which is an effective field theory that expands full quantum chromodynamics in inverse powers of a heavy-quark mass  $m$  Assi et al. [2023]. The bilinear heavy-quark Lagrangian  $\mathcal{L}$  up to  $O(1/m^3)$  reads,

$$\mathcal{L}_{\text{NRQCD}} = \psi^\dagger \left( iD_0 - m + \frac{D^2}{2m} + \frac{D^4}{8m^3} + c_F \frac{g\sigma B}{2m} + \dots \right) \psi, \quad (3)$$

where  $D$  represents the covariant derivative,  $\psi$  is the heavy quark field, and  $\frac{g\sigma B}{2m}$  is the term associated with chromomagnetic field interactions. Crucially, the  $\frac{D^4}{8m^3}$  operator acts as the leading positive quartic kinetic correction, ensuring the heavy-quark Hamiltonian remains bounded and stable with relativistic expansions Brambilla et al. [2000]. Further details on the stability provided by the quartic term is provided in Appendix A.

### 3 Method

To translate this physics insight into an optimizer design, we identify the stabilizing aspects of such phenomena such as the heavy-quark momentum with the optimizer’s global momentum buffer  $v$ . Accordingly, we posit a kinetic energy of the form:  $T_{\text{VRAdam}}(v) = \frac{m}{2}\|v\|^2 + \frac{\beta_3}{4}\|v\|^4$ , where  $m$  is the mass and  $\beta_3$  is a tunable parameter. The Lagrangian then becomes:

$$\mathcal{L}(x, v) = \frac{m}{2}v^2 + \frac{\beta_3}{4}v^4 - V(x), \quad (4)$$

where we solve for Euler-Lagrange equation:  $\frac{d}{dt} \frac{\partial \mathcal{L}}{\partial v} - \frac{\partial \mathcal{L}}{\partial x} = 0$ . Such that,

$$\frac{\partial \mathcal{L}}{\partial x} = -\frac{\partial V(x)}{\partial x} = -\nabla L_{\text{loss}}(x). \quad (5)$$

We know that the loss of a neural network with parameters  $x$  can be thought of as the potential landscape Holderrieth et al. [2024].

$$\begin{aligned} \frac{\partial \mathcal{L}}{\partial v} &= \frac{\partial T_{\text{VRAdam}}}{\partial v} = \frac{\partial}{\partial v} \left( \frac{1}{2}m\|v\|^2 + \frac{1}{4}\beta_3(\|v\|^2)^2 \right) \\ &= (m + \beta\|v\|^2)v \end{aligned} \quad (6)$$

The generalized momentum in this form is given by:

$$p = \frac{\partial L}{\partial v} = (m + \beta_3 \|v\|^2) v \quad (7)$$

The time derivative for the generalized momentum is then

$$\frac{d}{dt} \frac{\partial L}{\partial v} = \frac{d}{dt} [(m + \beta_3 \|v\|^2) v] \quad (8)$$

The Euler-Lagrange equation then becomes

$$\frac{d}{dt} [(m + \beta_3 \|v\|^2) v] = -\nabla L_{\text{Loss}}(x), \quad (9)$$

which can be rearranged to

$$\dot{v} = -\nabla L_{\text{Loss}}(x)/(m + 3\beta_3 \|v\|^2), \dot{x} = v \quad (10)$$

where the dot corresponds to the time derivative. Rather than explicitly constructing an optimizer based on an ordinary differential equation solver for Eq. 10 (via discretization and introduction of dissipation, e.g. França et al. [2020]), we utilize the term,  $(1/(m + 3\beta_3 \|v\|^2))$ , and embed it as a dynamic learning rate into AdamW, to enhance the successfully proven properties. In particular, this approach avoids choosing specific forms associated with various different integrators. The full velocity regularized Adam is given in Alg. 1, where we highlight in blue the changes to AdamW.

In Fig. 1, the vector field in Eq. 10 is plotted for the case of the loss function being a simple quadratic. Compared to kinetic energy term without quartic velocity, the vector field is “squeezed” in  $v$  direction, and the resulting trajectories are not circular. In this idealized setting, we can visualize the performance of VRAdam and Adam simplified to VRMomentum and Momentum, which corresponds to Alg. 1 without second-order moment estimates or bias corrections (setting  $m_t = 1$  and dropping lines 6, 8, and 9). After the first step, the lower step size of VRMomentum compared to Momentum can be seen, which leads to fewer oscillations.

**Algorithm 1** VRAdam optimizer.  $f(\theta)$ : objective function;  $\beta_1, \beta_2 \in [0, 1)$ ;  $v_t$ : velocity estimate;  $m_t$ : second-moment estimate;  $\eta_t$ : dynamic learning rate at step  $t$ ;  $\alpha_0$ : maximal learning rate;  $\alpha_0/(1 + \alpha_1)$ : minimal learning rate;  $\beta_3$ : velocity penalizer

---

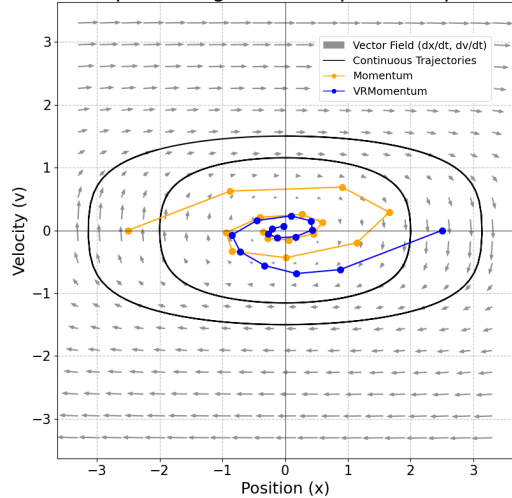
```

1: Input:  $f(\theta)$ ,  $\theta_0$ ,  $\alpha_0$ ,  $\alpha_1$ ,  $\beta_1$ ,  $\beta_2$ ,  $\beta_3$ ,  $\epsilon$ ,  $\lambda$ 
2: Initialize  $v_0 \leftarrow 0$ ,  $m_0 \leftarrow 0$ 
3: for  $t = 1, \dots, T$  do
4:    $g_t \leftarrow \nabla f(\theta_{t-1})$ 
5:    $v_t \leftarrow \beta_1 v_{t-1} + (1 - \beta_1) g_t$ 
6:    $m_t \leftarrow \beta_2 m_{t-1} + (1 - \beta_2) g_t^2$ 
7:    $\eta_t \leftarrow \alpha_0 / (1 + \min(\beta_3 \|v_t\|^2, \alpha_1))$ 
8:    $\hat{v}_t \leftarrow v_t / (1 - \beta_1^t)$ 
9:    $\hat{m}_t \leftarrow m_t / (1 - \beta_2^t)$ 
10:   $\theta_t \leftarrow \theta_{t-1} (1 - \eta_t \lambda) - \eta_t \frac{\hat{v}_t}{\sqrt{\hat{m}_t} + \epsilon}$ 
11: end for
12: Output:  $\theta_T$ 

```

---

Figure 1: Vector field  $\dot{v} = -x/(1 + 3v^2)$  and  $\dot{x} = v$  derived by solving the Euler-Lagrange equation for  $\mathcal{L} = v^2/2 + v^4/4 - x^2/2$ . Black lines are continuous trajectories; blue/orange show VRMomentum vs. Momentum steps.



For VRAdam, we obtain, through reparameterization and modification, the dynamic learning rate  $\eta_t = \alpha_0 / (1 + \min(\beta_3 \|v_t\|^2, \alpha_1))$  for timestep  $t$ , where  $\alpha_0$  and  $\alpha_1$  control the maximal and minimal LR respectively, and  $\beta_3$  as the velocity penalizer. This is inspired by the bound introduced to  $v^2$  in physical setting as discussed in Appendix A. The parameterization of LR, compared to the physically

derived one, clips the velocity to avoid getting stuck if gradients and therefore velocity become large. Furthermore, replacing the norm of the velocity (exponential moving average of gradients) with the current gradient norm (a more local property) can lead to improved performance in some scenarios. Weight decay is applied in the traditional manner.

## 4 Analysis

Here, we analyze the behavior of VRAdam in the adaptive edge of stability regime compared to that of Adam. For this analysis, following Cohen et al. [2024], we train a ResNet 32 architecture on CIFAR-10 for an image classification task, both with VRAdam and Adam. The training is stopped as soon as the training loss falls below 0.1 or an accuracy of 0.97 is reached. In Fig. 2 (a) and (b), the training curves of VRAdam indicate faster convergence in both minimizing training loss as well as maximizing training accuracy as compared to Adam. The training curves are smooth for both optimizers. When juxtaposed with the sharpness comparison depicted in Fig. 2 (c), we observe that the maximum eigenvalue (sharpness) of the preconditioned Hessian of the loss, remains consistently lower due to the dynamic learning rate adjustments induced by VRAdam. We can empirically observe that this “self-braking mechanism” enables VRAdam to operate in a regime of optimal lower sharpness and escape sharp oscillations, leading to faster convergence. (The negative eigenvalues are likely artifacts of the power method used to compute the largest eigenvalue [Trefethen and Bau, 1997].)

The effective learning rate of VRAdam is shown in Fig 2 (d). During the first 25 iterations, the learning rate dynamically increases close to the maximal value allowed LR and then proceeds to decrease while exhibiting oscillatory behavior as we converge to the minima. The bound on the minimal LR is not active in this example, while the base LR of Adam stays constant throughout training. As described in the seminal work of Schmidhuber *et al.*, we note that minima with lower sharpness are associated with better generalization Hochreiter and Schmidhuber [1997], Foret *et al.* [2021]. We can also observe, that VRAdam’s dynamic learning rate quickly moves to the maximal LR to exploit the loss landscape optimally, while exploiting the trade-off between the adaptive edge of stability and faster convergence.

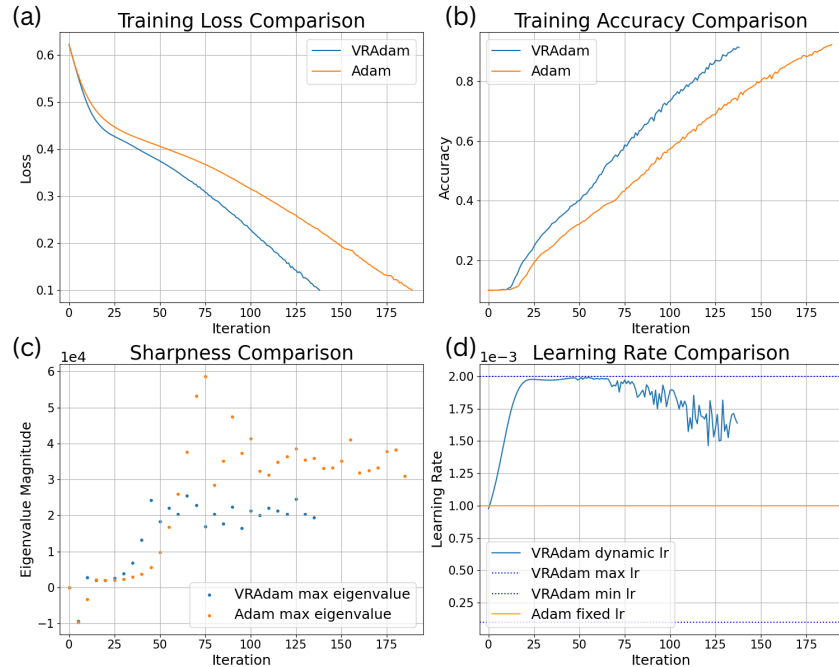


Figure 2: **(a)** Training loss curves for VRAdam and Adam of ResNet 32 on CIFAR-10 **(b)** training accuracy curves **(c)** plot of maximal eigenvalues of the loss Hessian **d** effective learning rate during training. Hyperparameters for these plots are provided in Appendix B.5.

## 5 Benchmarks

We benchmark VRAdam against various optimizers on several datasets for various tasks with diverse architectures. These benchmarks include image classification using a CNN on the CIFAR-10 dataset Krizhevsky and Hinton [2009], language modelling with a Transformer architecture Vaswani et al. [2023] on the WikiText2 dataset Merity et al. [2016], and Generative Flow Networks (GFLowNets) Avidan et al. [2025], on a grid world for sequence generation tasks Chevalier-Boisvert et al. [2023]. We also report hyperparameter sensitivity on a diffusion model trained through an UNet architecture Petit et al. [2021] with self attention modules placed in the bottle neck and upper layers for the handwritten digit dataset MNIST LeCun et al. [1998]. These benchmarks represent a broad variety of deep learning architectures and tasks, ranging from older techniques for image classification to much **newer and actively emerging** models and training techniques such as for GFLowNets. We focus on the comparison with AdamW since its exceeding popularity and consistent performance but also report the performance of stochastic gradient descent (SGD) with momentum [Qian, 1999] and root mean square propagation (RMSProp) Ruder [2017]. In particular, we demonstrate the **excellent convergence** properties as well performance improvements in most benchmarks for VRAdam. Note that we run *Bayesian optimization for hyperparameter sweeps* for the image classification, language modeling and diffusion modeling tasks, with several evaluations in close proximity to the found minimum, and the results are statistically significant. We report the optimal value from this optimization procedure, however, we include shaded error bars in the appendix. The Bayesian optimization for the hyperparameters was conducted with the objective to minimize validation loss, however, we also report test loss. Hyperparameters for the task involving GFlowNets were picked at random due compute constraints. All details regarding model training, setup and datasets along with error envelopes using multiple runs are provided in Appendices B and D.

### 5.1 Image classification

Image classification serves as a foundational benchmark for deep learning optimizers. This task evaluates VRAdam’s ability to navigate complex, non-convex loss landscapes typical of convolutional neural networks (CNNs) and to achieve good generalization on unseen data. The CIFAR-10 dataset comprises 60,000 32x32 color images categorized into 10 distinct classes, with 6,000 images per class. The dataset is conventionally partitioned into 50,000 images for training and 10,000 for testing. Input images are preprocessed with a normalization scheme based on the per-channel mean and standard deviation of the CIFAR-10 dataset. During training, data augmentation techniques are applied to enhance model robustness and reduce overfitting; these include random horizontal flips and random crops.

The CNN consists of a feature extractor that utilizes three sequential convolutional blocks, where each block contains two 3x3 convolutional layers, each followed by batch normalization and ReLU activation, and concludes with a 2x2 max-pooling operation. These blocks progressively increase the channel depth while reducing the spatial dimensions of the feature maps. The resulting feature maps are then flattened and passed to a classifier module. This classifier comprises a fully-connected layer with a ReLU activation, followed by a final fully-connected layer that outputs logits for the 10 CIFAR-10 classes. Optimizers are tasked with minimizing the Cross-Entropy Loss, a standard loss function for multi-class classification Mao et al. [2023].

Method	Validation Loss	Test Loss
VRAdam	<b>0.476</b>	<b>0.469</b>
AdamW	0.522	0.565
SGD+Nesterov	0.625	0.620
RMSProp	0.801	0.813

Table 1: Image classification results of optimizers on CIFAR-10 reported through model loss.

### 5.2 Language modeling

Language modeling is a core task in natural language processing, requiring models to capture complex dependencies and contextual information within sequential data. Here, we assess how well VRAdam

compares to other optimizers in training large Transformer models for language modeling. The WikiText-2 dataset, a corpus of over 100 million tokens from Wikipedia articles, is used. The preprocessing step involves data tokenization, and sequence construction.

The Transformer used is a standard encoder-decoder architecture with embedding layers, positional encoding, multi-head attention, and feed-forward networks. The training objective is next-token prediction, where optimizers work to minimize the Cross-Entropy Loss between the model’s predictions and the actual subsequent tokens, with padding tokens ignored during loss calculation. We report NaNs for SGD with momentum and Nesterov, as well as RMSProp due to well-known numerical instability across multiple hyperparameter sweeps Liu et al. [2023b], Vashisht and Ramaswamy [2023], Popel and Bojar [2018].

Method	Validation Loss	Test Loss
VRAdam	<b>5.99</b>	<b>6.00</b>
AdamW	6.47	6.50
SGD+Nesterov	NaN	NaN
RMSProp	NaN	NaN

Table 2: Language modeling results of optimizers on WikiText-2 reported through model loss.

### 5.3 GFlowNets on GridWorld

This benchmark evaluates the performance of VRAdam on a distinct generative task using GFlowNets. GFlowNets are a class of probabilistic models adept at learning to sample complex, discrete objects  $x$  (such as sequences of actions leading to grid patterns) from a target distribution  $P^*(x)$  that is proportional to a given non-negative reward function  $R(x)$ , i.e.,  $P^*(x) \propto R(x)$ . Unlike traditional reinforcement learning (RL) approaches that often converge to a policy maximizing expected reward (potentially collapsing to a single mode), GFlowNets are designed to learn to sample a diversity of high-reward candidates, making them particularly well-suited for tasks where exploring multiple solutions is crucial. This benchmark tests an ability of an optimizer to handle the unique training objectives of GFlowNets, which involve learning a stochastic forward policy  $P_F(a_t|s_t; \theta)$  to construct objects step-by-step, and often an auxiliary backward policy  $P_B(s_{t-1}|s_t; \phi)$  and a flow function  $F(s; \psi)$  over a structured state space  $\mathcal{S}$ .

The specific goal is to train a GFlowNet, parameterized by  $\theta, \phi, \psi$ , to learn a policy that constructs patterns on an  $8 \times 8$  grid. An object is formed by a trajectory of states and actions  $\tau = (s_0, a_0, s_1, \dots, s_T)$ , where  $s_t \in \mathcal{S}$  is the state at step  $t$  (representing the grid, agent position, and visitation map) and  $a_t \in \mathcal{A} = \{\text{up, down, left, right, stop}\}$  is the action taken. The GFlowNet, includes a CNN-based grid encoder and MLP-based policy and flow networks, aims to generate trajectories  $\tau$  such that the final state  $s_T$  is sampled proportionally to a complex reward  $R(s_T)$ . This reward, considers the geometric patterns formed, overall grid coverage, generation efficiency (penalizing redundant actions), and symmetry of the final configuration. The optimizers are used to minimize a composite GFlowNet loss function  $\mathcal{L}_{\text{GFN}}$ , which includes:

1. **A Flow Matching or Trajectory Balance Loss ( $\mathcal{L}_{\text{FM}}$ )**: This core component ensures that the learned policy and flow function are internally consistent. This loss component aims to satisfy a detailed balance-like condition, minimizing the squared difference between forward flows  $F(s_t; \psi)P_F(a_t|s_t; \theta)$  and backward flows  $F(s_{t+1}; \psi)P_B(s_t|s_{t+1}; \phi)$  for transitions  $(s_t, a_t, s_{t+1})$  in sampled trajectories. It also includes a term to match the flow of terminal states  $F(s_T; \psi)$  to their rewards  $R(s_T)$ .
2. **A Reward Loss Component ( $\mathcal{L}_R$ ) and a Entropy Regularization Term ( $\mathcal{L}_H$ )** for the policy: These term directly encourage the generation of high-reward states and exploration respectively.

The total loss is a weighted sum:  $\mathcal{L}_{\text{GFN}} = w_{\text{FM}}\mathcal{L}_{\text{FM}} + w_R\mathcal{L}_R + w_H\mathcal{L}_H$ , where  $w_{\text{FM}}, w_R, w_H$  are scalar weight. Performance is primarily evaluated by the final flow matching loss, which indicates how well the GFlowNet has learned the target distribution.

Method	Validation Flow Loss	Test Flow Loss
VRAdam	<b>1.25</b>	<b>1.33</b>
AdamW	2.41	3.6
SGD+Nesterov	2.71	2.61
RMSProp	25.0	25.0

Table 3: GFlowNets results of optimizers on GridWorld reported through flow match loss.

#### 5.4 Hyperparameter Sensitivity of Diffusion Models for Generative Modeling

Diffusion models have emerged as powerful generative models, particularly for high-fidelity image and video synthesis. However, their training can be computationally intensive and sensitive to hyperparameter choices. This benchmark assesses the robustness of VRAdam and the ease of finding effective hyperparameter settings when training a diffusion model. The dataset consists of  $28 \times 28$  grayscale MNIST images.

The diffusion trading process involves a forward noising process and a learned reverse denoising process. The reverse process, which generates images by iteratively removing noise, is powered by a UNet architecture with self-attention. This U-Net is specifically designed for diffusion tasks, incorporating time embeddings (derived from sinusoidal positional encodings processed by an MLP) that allow the network to condition its predictions on the current noise level (timestep). For these benchmarks, this U-Net due to its self-attention mechanism effectively captures global image context and long-range dependencies, which are vital for generating coherent images.

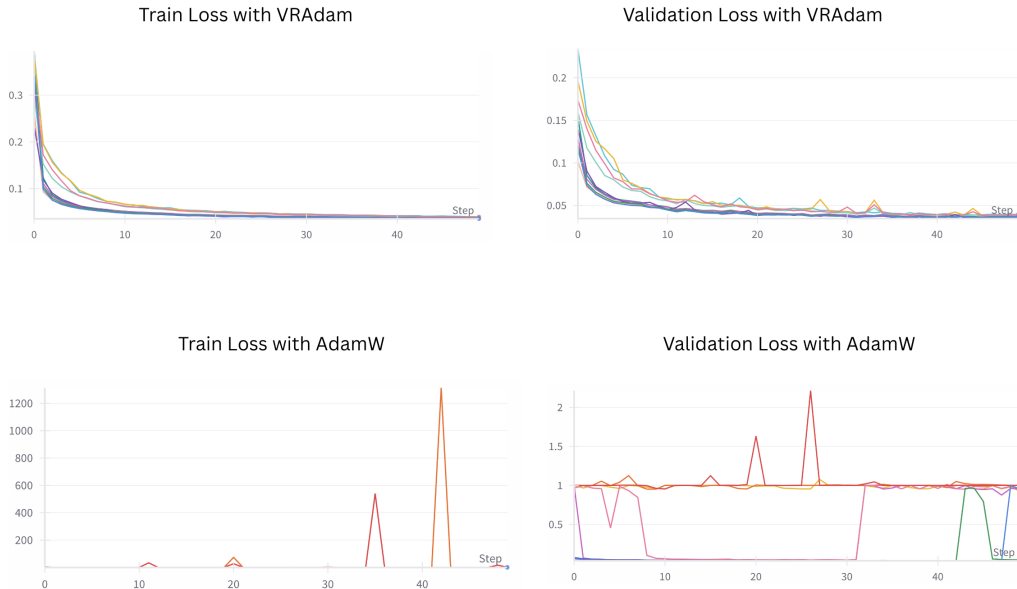


Figure 3: The mean squared error (MSE) training and validation loss over ten sweeps of hyperparameters using Bayesian optimization for a generative modeling task using a Transformer optimized with VRAdam and AdamW for [Hyperparameter in the appendix].

Crucially as seen in Fig. 3, we highlight the **robustness** of VRAdam to various hyperparameter choices during multiple sweeps by reporting the training and validation loss. VRdam demonstrates significantly more stable and robust performance than AdamW for training this diffusion model, with far smoother convergence. In contrast, AdamW exhibits widespread instability, with many hyperparameter settings leading to erratic training, failure to converge Karras et al. [2022], even as some specific choices lead to comparable performance to that of VRAdam. This robust performance across a wide range of its hyperparameters suggests that VRdam can achieve satisfactory results with **minimal tuning**, and potentially even with its default settings, thereby reducing the need for

extensive hyperparameter searches. We also provide the details regarding the performance of SGD and RMSProp in the appendix.

## 6 Related Work

**Follow-up work on Adam** The Adam optimizer was introduced in 2014 by Kingma and Ba [2017] by combining the previously existing concepts of momentum and scaling a base LR for each parameter based on second-order moment estimates. The base learning rate, however, remains hard-coded (potentially chosen through a learning rate scheduler) throughout training. Since then, several modifications to Adam have been introduced, such as NAdam Dozat [2016], RAdam Liu et al., Adabelief Zhuang et al. [2020], and in particular AdamW Loshchilov and Hutter, which reintroduces weight decay in its original intention. LARS You et al. [2017] and LAMB You et al. [2020] compute learning rates for layers individually. More recent optimization techniques include LION, an automatically discovered alternative to signed momentum Chen et al. [2023], Sophia Liu et al. [2023a], which uses estimated diagonal entries of the Hessian as a precondition, sharpness-aware minimization methods Foret et al. [2021], and a modified LR in Adam for reinforcement learning Ellis et al. [2024].

**Understanding training dynamics, convergence analysis, and edge of stability** Another line of work focuses on understanding the dynamics of the training of deep neural networks as well as derive convergence properties and guarantees for commonly used optimizers. Wang and Choromanska [2025] provides a recent survey over the later and Reddi et al. [2019] provide an explicit convex example for which Adam does not converge. A popularized framework for understanding training dynamics in the continuous training flow and infinite network width limit was introduced in Jacot et al. [2018], extended by finite width corrections in Huang and Yau [2020], and developed for graph neural networks in Du et al. [2019]. Lastly, the role of the edge of stability regime offers an empirically view and was analyzed in Cohen et al. [2024], Arora et al. [2022], Cohen et al. [2022], Damian et al. [2022], Song and Yun [2023], Wang et al. [2022]

**Symplectic Optimization** This research area derives discrete-time optimization algorithms by discretizing continuous-time Hamiltonian or Lagrangian flows using symplectic integrators, which exactly preserve the underlying geometric (symplectic) structure of the dynamical system. This approach guarantees long-term stability, energy-preservation properties (or controlled energy dissipation in the dissipative case), and can provide valuable insights into existing optimizers. Notable work includes Betancourt et al. [2018], França et al. [2020], Maddison et al. [2018], Duruisseaux and Leok [2023], Yuan and Zhang [2023].

## 7 Discussion

**Limitations** We note that due to limited compute resources we were not able to benchmark the performance of VRAdam on model sizes beyond 56 million parameters. The edge of stability regime remains not fully understood and questions regarding generalization capabilities remain.

**Summary of work** Motivated by physical perspectives for complex optimization scenarios and stability conditions along with the adaptive edge of stability, we developed a new optimizer VRAdam based on quartic kinetic energy terms. We analyzed its performance at the adaptive edge of stability and benchmark it against several optimizers in particular AdamW on image classification, language modeling, a generative task using GFlowNets as well as diffusion modeling where we report improved performance and robustness to hyperparameters.

**Future work** We hope that this work leads to further development of sophisticated and interpretable optimizers using concepts from physics, since even small improvement can lead to significant savings in resources.

## References

- David H. Ackley, Geoffrey E. Hinton, and Terrence J. Sejnowski. A learning algorithm for boltzmann machines. *Cognitive Science*, 9(1):147–169, 1985.

- Sanjeev Arora, Zhiyuan Li, and Abhishek Panigrahi. Understanding gradient descent on edge of stability in deep learning, 2022. URL <https://arxiv.org/abs/2205.09745>.
- Benoît Assi, Bernd A. Kniehl, and Joan Soto. Matching the standard model to heavy-quark effective theory and nonrelativistic qcd. *Nuclear Physics B*, 992:116173, July 2023. ISSN 0550-3213. doi: 10.1016/j.nuclphysb.2023.116173. URL <http://dx.doi.org/10.1016/j.nuclphysb.2023.116173>.
- Yehonatan Avidan, Qianyi Li, and Haim Sompolinsky. Connecting ntk and nngp: A unified theoretical framework for wide neural network learning dynamics, 2025. URL <https://arxiv.org/abs/2309.04522>.
- Michael Betancourt, Michael I. Jordan, and Ashia C. Wilson. On symplectic optimization. *arXiv preprint arXiv:1802.03653*, 2018.
- Stephen Boyd and Lieven Vandenberghe. *Convex optimization*. Cambridge university press, 2004.
- Eric Braaten. Introduction to the nrqcd factorization approach to heavy quarkonium, 1997. URL <https://arxiv.org/abs/hep-ph/9702225>.
- Nora Brambilla, Antonio Pineda, Joan Soto, and Antonio Vairo. Potential nrqcd: an effective theory for heavy quarkonium. *Nuclear Physics B*, 566(1–2):275–310, January 2000. ISSN 0550-3213. doi: 10.1016/s0550-3213(99)00693-8. URL [http://dx.doi.org/10.1016/S0550-3213\(99\)00693-8](http://dx.doi.org/10.1016/S0550-3213(99)00693-8).
- Xiangning Chen, Chen Liang, Da Huang, Esteban Real, Kaiyuan Wang, Hieu Pham, Xuanyi Dong, Thang Luong, Cho-Jui Hsieh, Yifeng Lu, et al. Symbolic discovery of optimization algorithms. *Advances in neural information processing systems*, 36:49205–49233, 2023.
- Maxime Chevalier-Boisvert, Bolun Dai, Mark Towers, Rodrigo Perez-Vicente, Lucas Willems, Salem Lahlou, Suman Pal, Pablo Samuel Castro, and Jordan Terry. Minigrid & miniworld: Modular & customizable reinforcement learning environments for goal-oriented tasks. In *Advances in Neural Information Processing Systems 36, New Orleans, LA, USA*, December 2023.
- Jeremy M. Cohen, Simran Kaur, Yuanzhi Li, J. Zico Kolter, and Ameet Talwalkar. Gradient descent on neural networks typically occurs at the edge of stability, 2022. URL <https://arxiv.org/abs/2103.00065>.
- Jeremy M. Cohen, Behrooz Ghorbani, Shankar Krishnan, Naman Agarwal, Sourabh Medapati, Michal Badura, Daniel Suo, David Cardoze, Zachary Nado, George E. Dahl, and Justin Gilmer. Adaptive gradient methods at the edge of stability, 2024. URL <https://arxiv.org/abs/2207.14484>.
- Alex Damian, Eshaan Nichani, and Jason D Lee. Self-stabilization: The implicit bias of gradient descent at the edge of stability. *arXiv preprint arXiv:2209.15594*, 2022.
- Timothy Dozat. Incorporating nesterov momentum into adam. 2016.
- Simon S Du, Kangcheng Hou, Russ R Salakhutdinov, Barnabas Poczos, Ruosong Wang, and Keyulu Xu. Graph neural tangent kernel: Fusing graph neural networks with graph kernels. *Advances in neural information processing systems*, 32, 2019.
- Valentin Duruisseaux and Melvin Leok. Practical perspectives on symplectic accelerated optimization. *Optimization Methods and Software*, 38(6):1230–1268, 2023. doi: 10.1080/10556788.2023.2214837.
- Benjamin Ellis, Matthew T Jackson, Andrei Lupu, Alexander D Goldie, Mattie Fellows, Shimon Whiteson, and Jakob Foerster. Adam on local time: Addressing nonstationarity in rl with relative adam timesteps. *Advances in Neural Information Processing Systems*, 37:134567–134590, 2024.
- Pierre Foret, Ariel Kleiner, Hossein Mobahi, and Behnam Neyshabur. Sharpness-aware minimization for efficiently improving generalization. In *Advances in Neural Information Processing Systems (NeurIPS)*, 2021.

Guilherme Fran  a, Jeremias Sulam, Daniel Robinson, and Ren   Vidal. Conformal symplectic and relativistic optimization. *Advances in Neural Information Processing Systems*, 33:16916–16926, 2020.

Partha Guha and A Ghose-Choudhury. Construction of the classical time crystal lagrangians from sisyphus dynamics and duality description with the li  nard type equation, 2019. URL <https://arxiv.org/abs/1911.11626>.

Sepp Hochreiter and J  rgen Schmidhuber. Flat minima. *Neural Computation*, 9(1):1–42, 1997. doi: 10.1162/neco.1997.9.1.1.

Peter Holderrieth, Yilun Xu, and Tommi Jaakkola. Hamiltonian score matching and generative flows, 2024. URL <https://arxiv.org/abs/2410.20470>.

John J. Hopfield. Neural networks and physical systems with emergent collective computational abilities. *Proceedings of the National Academy of Sciences*, 79(8):2554–2558, 1982.

Jiaoyang Huang and Horng-Tzer Yau. Dynamics of deep neural networks and neural tangent hierarchy. In *International conference on machine learning*, pages 4542–4551. PMLR, 2020.

Arthur Jacot, Franck Gabriel, and Cl  ment Hongler. Neural tangent kernel: Convergence and generalization in neural networks. *Advances in neural information processing systems*, 31, 2018.

Tero Karras, Miika Aittala, Timo Aila, and Samuli Laine. Elucidating the design space of diffusion-based generative models, 2022. URL <https://arxiv.org/abs/2206.00364>.

Diederik P. Kingma and Jimmy Ba. Adam: A method for stochastic optimization, 2017. URL <https://arxiv.org/abs/1412.6980>.

Alex Krizhevsky and Geoffrey E. Hinton. Learning multiple layers of features from tiny images. Technical Report TR-2009-003, University of Toronto, 2009. URL <https://www.cs.toronto.edu/~kriz/learning-features-2009-TR.pdf>.

Yann LeCun, L  on Bottou, Yoshua Bengio, and Patrick Haffner. Gradient-based learning applied to document recognition. *Proceedings of the IEEE*, 86(11):2278–2324, 1998.

Hong Liu, Zhiyuan Li, David Hall, Percy Liang, and Tengyu Ma. Sophia: A scalable stochastic second-order optimizer for language model pre-training. *arXiv preprint arXiv:2305.14342*, 2023a.

Liyuan Liu, Haoming Jiang, Pengcheng He, Weizhu Chen, Xiaodong Liu, Jianfeng Gao, and Jiawei Han. On the variance of the adaptive learning rate and beyond. In *International Conference on Learning Representations*.

Liyuan Liu, Xiaodong Liu, Jianfeng Gao, Weizhu Chen, and Jiawei Han. Understanding the difficulty of training transformers, 2023b. URL <https://arxiv.org/abs/2004.08249>.

Ilya Loshchilov and Frank Hutter. Decoupled weight decay regularization. In *International Conference on Learning Representations*.

Chris J. Maddison, Daniel Paulin, Yee Whye Teh, Brendan O’Donoghue, and Arnaud Doucet. Hamiltonian descent methods. *arXiv preprint arXiv:1809.05042*, 2018.

Anqi Mao, Mehryar Mohri, and Yutao Zhong. Cross-entropy loss functions: Theoretical analysis and applications, 2023. URL <https://arxiv.org/abs/2304.07288>.

Stephen Merity, Caiming Xiong, James Bradbury, and Richard Socher. Pointer sentinel mixture models, 2016.

Antti J. Niemi. Time crystals: From schr  dinger to sisyphus, 2021. URL <https://arxiv.org/abs/2109.06091>.

Olivier Petit, Nicolas Thome, Cl  ment Rambour, and Luc Soler. U-net transformer: Self and cross attention for medical image segmentation, 2021. URL <https://arxiv.org/abs/2103.06104>.

- Martin Popel and Ondřej Bojar. Training tips for the transformer model. *The Prague Bulletin of Mathematical Linguistics*, 110(1):43–70, April 2018. ISSN 1804-0462. doi: 10.2478/pralin-2018-0002. URL <http://dx.doi.org/10.2478/pralin-2018-0002>.
- Ning Qian. On the momentum term in gradient descent learning algorithms. *Neural Networks*, 12(1):145–151, 1999. ISSN 0893-6080. doi: [https://doi.org/10.1016/S0893-6080\(98\)00116-6](https://doi.org/10.1016/S0893-6080(98)00116-6). URL <https://www.sciencedirect.com/science/article/pii/S0893608098001166>.
- Sashank J Reddi, Satyen Kale, and Sanjiv Kumar. On the convergence of adam and beyond. *arXiv preprint arXiv:1904.09237*, 2019.
- Sebastian Ruder. An overview of gradient descent optimization algorithms, 2017. URL <https://arxiv.org/abs/1609.04747>.
- Alfred Shapere and Frank Wilczek. Classical time crystals. *Physical Review Letters*, 109(16), October 2012. ISSN 1079-7114. doi: 10.1103/physrevlett.109.160402. URL <http://dx.doi.org/10.1103/PhysRevLett.109.160402>.
- Minhak Song and Chulhee Yun. Trajectory alignment: understanding the edge of stability phenomenon via bifurcation theory. *arXiv preprint arXiv:2307.04204*, 2023.
- Ilya Sutskever, James Martens, George Dahl, and Geoffrey Hinton. On the importance of initialization and momentum in deep learning. In *International conference on machine learning*, pages 1139–1147. PMLR, 2013.
- Lloyd N. Trefethen and David Bau. *Numerical Linear Algebra*. SIAM, 1997. ISBN 0898713617.
- Rahul Vashisht and Harish G. Ramaswamy. *On the Learning Dynamics of Attention Networks*. IOS Press, September 2023. ISBN 9781643684376. doi: 10.3233/FAIA230541. URL <http://dx.doi.org/10.3233/FAIA230541>.
- Ashish Vaswani, Noam Shazeer, Niki Parmar, Jakob Uszkoreit, Llion Jones, Aidan N. Gomez, Łukasz Kaiser, and Illia Polosukhin. Attention is all you need, 2023. URL <https://arxiv.org/abs/1706.03762>.
- Jing Wang and Anna Choromanska. A survey of optimization methods for training dl models: Theoretical perspective on convergence and generalization, 2025. URL <https://arxiv.org/abs/2501.14458>.
- Zixuan Wang, Zhouzi Li, and Jian Li. Analyzing sharpness along gd trajectory: Progressive sharpening and edge of stability. *Advances in Neural Information Processing Systems*, 35:9983–9994, 2022.
- Yang You, Igor Gitman, and Boris Ginsburg. Large batch training of convolutional networks, 2017. URL <https://arxiv.org/abs/1708.03888>.
- Yang You, Jing Li, Sashank Reddi, Jonathan Hseu, Sanjiv Kumar, Srinadh Bhojanapalli, Xiaodan Song, James Demmel, Kurt Keutzer, and Cho-Jui Hsieh. Large batch optimization for deep learning: Training bert in 76 minutes, 2020. URL <https://arxiv.org/abs/1904.00962>.
- Ya-xiang Yuan and Yi Zhang. Symplectic discretization approach for developing new proximal point algorithm. *arXiv preprint arXiv:2308.03986*, 2023.
- Juntang Zhuang, Tommy Tang, Yifan Ding, Sekhar C Tatikonda, Nicha Dvornek, Xenophon Papademetris, and James Duncan. Adabelief optimizer: Adapting stepsizes by the belief in observed gradients. *Advances in neural information processing systems*, 33:18795–18806, 2020.

## A Bounding NRQCD

Starting with the NRQCD Lagrangian density in Euclidean space:

$$\mathcal{L}_{\text{NRQCD}} = \psi^\dagger \left( iD_0 - m + \frac{\mathbf{D}^2}{2m} + \frac{\mathbf{D}^4}{8m^3} + \dots \right) \psi \quad (11)$$

The corresponding Hamiltonian density is derived via Legendre transformation:

$$\mathcal{H}_{\text{NRQCD}} = \psi^\dagger \left( m - \frac{\mathbf{D}^2}{2m} - \frac{\mathbf{D}^4}{8m^3} - \dots \right) \psi \quad (12)$$

For a rigorous analysis of the dispersion relation, we work in momentum space:

$$\psi(\vec{x}, t) = \int \frac{d^3 p}{(2\pi)^3} e^{i\vec{p} \cdot \vec{x}} \tilde{\psi}(\vec{p}, t) \quad (13)$$

In momentum space, the operators transform as:

$$D_0 \rightarrow -iE \quad (\text{time evolution operator}) \quad (14)$$

$$\mathbf{D} \rightarrow i\vec{p} \quad (\text{spatial covariant derivative}) \quad (15)$$

$$\mathbf{D}^2 \rightarrow -p^2 \quad (\text{squared spatial derivative}) \quad (16)$$

$$\mathbf{D}^4 \rightarrow p^4 \quad (\text{quartic spatial derivative}) \quad (17)$$

The energy eigenvalue equation derived from the Hamiltonian is:

$$E\tilde{\psi}(\vec{p}) = \left( m + \frac{p^2}{2m} - \frac{p^4}{8m^3} + \mathcal{O}\left(\frac{1}{m^5}\right) \right) \tilde{\psi}(\vec{p}) \quad (18)$$

This gives the NRQCD dispersion relation to order  $1/m^3$ :

$$E_{\text{NRQCD}}(p) = m + \frac{p^2}{2m} - \frac{p^4}{8m^3} + \mathcal{O}\left(\frac{1}{m^5}\right) \quad (19)$$

### A.1 Analysis of Boundedness

The exact relativistic energy-momentum relation:

$$E_{\text{rel}}(p) = \sqrt{m^2 + p^2} \quad (20)$$

Using Taylor series expansion for  $\sqrt{1+x}$  where  $x = p^2/m^2$ :

$$\sqrt{1+x} = 1 + \frac{1}{2}x - \frac{1}{8}x^2 + \frac{1}{16}x^3 - \frac{5}{128}x^4 + \mathcal{O}(x^5) \quad (21)$$

Applying this to the relativistic energy:

$$E_{\text{rel}}(p) = m \left( 1 + \frac{1}{2} \frac{p^2}{m^2} - \frac{1}{8} \frac{p^4}{m^4} + \mathcal{O}\left(\frac{p^6}{m^6}\right) \right) \quad (22)$$

Simplifying:

$$E_{\text{rel}}(p) = m + \frac{p^2}{2m} - \frac{p^4}{8m^3} + \mathcal{O}\left(\frac{p^6}{m^5}\right) \quad (23)$$

For the non-relativistic approximation without the quartic term:

$$\lim_{p \rightarrow \infty} \frac{E_{\text{NR}}(p)}{E_{\text{rel}}(p)} = \lim_{p \rightarrow \infty} \frac{m + \frac{p^2}{2m}}{\sqrt{m^2 + p^2}} \quad (24)$$

$$= \lim_{p \rightarrow \infty} \frac{m + \frac{p^2}{2m}}{\frac{p}{\sqrt{1 + \frac{m^2}{p^2}}}} \quad (25)$$

$$= \infty \quad (26)$$

This shows that the non-relativistic approximation without the quartic term diverges from the true relativistic behavior.

The quartic term introduces a negative contribution to the energy that precisely cancels the fourth-order term in the relativistic expansion:

$$E_{\text{NRQCD}}(p) = m + \frac{p^2}{2m} - \frac{p^4}{8m^3} + \mathcal{O}\left(\frac{1}{m^5}\right) \quad (27)$$

Let's define a parameter  $\lambda = p^2/m^2$  (proportional to  $v^2$ ). For the NRQCD expansion to be valid, we require  $\lambda \ll 1$ .

The second derivative of the NRQCD energy with respect to  $\lambda$  is:

$$\frac{d^2 E_{\text{NRQCD}}}{d\lambda^2} = -\frac{3m}{4}\lambda + \mathcal{O}(\lambda^2) \quad (28)$$

This becomes negative for sufficiently large  $\lambda$  within the domain of validity, indicating that the energy function develops a maximum rather than increasing unboundedly.

## B Hyperparameters, Datasets and Model Architectures

### B.1 Image Classification

This section details the comprehensive sweep for the CNN, on the CIFAR-10 dataset.

- Model: Convolutional Neural Network
- Dataset: CIFAR-10
- Hyperparameter sweep method: Bayesian optimization
- Optimization metric: validation loss

Table 4: Dataset Splits during CNN Sweep

Dataset Split	Configuration Description
Training	80% of the original CIFAR10 training set (50,000 images).
Validation	20% of the original CIFAR10 training set.
Test	Full CIFAR10 test set (10,000 images).

### B.2 Language Modeling

This section details the comprehensive sweep for the Transformer, on the WikiText-2 dataset.

- Model: Transformer
- Dataset: Wikitext-2
- Hyperparameter sweep method: Bayesian optimization
- Optimization metric: validation loss

Table 5: Fixed Hyperparameters during CNN Comprehensive Sweep

Parameter	Value
Model Architecture	Convolutional Neural Network
Dataset	CIFAR-10
Epochs	100
Batch Size	1024
Scheduler Type	WarmupCosineAnnealing
Warmup Epochs	5
Warmup Factor	0.1
Scheduler $\eta$ min	$1 \times 10^{-5}$
VRAdam $\beta_1$	0.9
VRAdam $\beta_2$	0.999
VRAdam power	2
VRAdam weight decay	$1 \times 10^{-5}$
VRAdam $\epsilon$	$1 \times 10^{-8}$
AdamW $\beta_1$	0.9
AdamW $\beta_2$	0.999
AdamW weight decay	$1 \times 10^{-5}$
SGD momentum	0.9
SGD nesterov	True
SGD weight decay	$1 \times 10^{-5}$
RMSProp $\alpha$	0.99
RMSProp	$1 \times 10^{-8}$
RMSProp weight decay	$1 \times 10^{-5}$

Table 6: Swept Hyperparameters during CNN Comprehensive Sweep

Optimizer	Parameter	Sweep Configuration	Optimal Parameter
VRAdam	$\eta$	Log-uniform, Min: $1 \times 10^{-4}$ , Max: 0.1	0.0846
VRAdam	$\beta_3$	Uniform, Min: 0.1, Max: 1.5	1.015
VRAdam	normgrad	Values: [True, False]	True
VRAdam	lr cutoff	Integer Uniform, Min: 3, Max: 30	29
AdamW	$\eta$	Log-uniform, Min: $1 \times 10^{-5}$ , Max: $1 \times 10^{-1}$	0.0625
SGD	$\eta$	Log-uniform, Min: $1 \times 10^{-5}$ , Max: $1 \times 10^{-1}$	0.00784
RMSProp	$\eta$	Log-uniform, Min: $1 \times 10^{-5}$ , Max: 0.1	1.78e-4

Table 7: Dataset Splits during Transformer Comprehensive Sweep

Dataset Split	Configuration Description
Training	Full WikiText-2 predefined training set.
Validation	Full WikiText-2 predefined validation set.
Test	Full WikiText-2 predefined test set.

### B.3 Generative Modeling with Diffusion

This section details the comprehensive sweep for the diffusion model, on the MNIST dataset.

- Model: UNet with self-attention
- Dataset: MNIST
- Hyperparameter sweep method: Bayesian optimization
- Optimization metric: validation loss

### B.4 Generative Modeling with GFlowNets

Here we include the hyperparameters used for reporting the performance of the optimizers for the GFlowNet.

Table 8: Fixed Hyperparameters during Transformer Comprehensive Sweep

Parameter	Value
Model Architecture	TransformerModel
Epochs	100
Batch Size	32
Seed	0
Scheduler Type	WarmupCosineAnnealing
Warmup Epochs	5
Warmup Factor	0.1
Scheduler $\eta$	$1 \times 10^{-5}$
Model sequence length	64
Model embed dimension	128
Model hidden dimension	256
VRAdam $\beta_1$	0.9
VRAdam $\beta_2$	0.999
VRAdam power	2
VRAdam weight decay	$1 \times 10^{-5}$
VRAdam $\epsilon$	$1 \times 10^{-8}$
AdamW $\beta_1$	0.9
AdamW $\beta_2$	0.999
AdamW weight decay	$1 \times 10^{-5}$
SGD sgd momentum	0.9
SGD sgd nesterov	True
RMSProp $\alpha$	0.1
RMSProp $\epsilon$	$1 \times 10^{-8}$

Table 9: Swept Hyperparameters during Transformer Comprehensive Sweep

Optimizer	Parameter	Sweep Configuration	Optimal Parameter
VRAdam	$\eta$	Log-uniform, Min: $1 \times 10^{-5}$ , Max: 0.1	1.55e-05
VRAdam	$\beta_3$	Uniform, Min: 0.1, Max: 5.0	3.35
VRAdam	normgrad	Values: [True, False]	False
VRAdam	lr cutoff	Integer Uniform, Min: 5, Max: 30	7
Adam	$\eta$	Log-uniform, Min: $1 \times 10^{-5}$ , Max: 0.1	1.661e-05
SGD	$\eta$	Log-uniform, Min: $1 \times 10^{-5}$ , Max: $1 \times 10^{-1}$	-
RMSProp	$\eta$	Log-uniform, Min: $1 \times 10^{-5}$ , Max: 0.1	-

Table 10: Dataset Splits during Diffusion Comprehensive Sweep

Dataset Split	Configuration Description
Training	90% of the original MNIST training set (60,000 images).
Validation	10% of the original MNIST training set.
Test	Full MNIST test set (10,000 images).

Table 14: Hyperparameters GFlowNets

Optimizer	Parameter	Value
VRAdam	$\eta$	0.01
VRAdam	$\beta_3$	1
VRAdam	normgrad	False
VRAdam	lr cutoff	19
VRAdam	weight decay	$1 \times 10^{-5}$
AdamW	weight decay	$1 \times 10^{-5}$
AdamW	$\eta$	0.01
SGD	$\eta$	0.01
RMSProp	$\eta$	0.01

Table 11: Fixed Hyperparameters during Diffusion Comprehensive Sweep

Parameter	Value
Seed	42
Epochs	50
Batch Size	128
UNet base channels	96
UNet time embed dim	128
UNet use attention	True
Diffusion num timesteps	400
Diffusion $\beta_{min}$	$1 \times 10^{-4}$
Diffusion $\beta_{max}$	0.02
Sample Every (sample every)	5 epochs
Optimizer weight decay (Common)	$1 \times 10^{-5}$
Adam/VRAdam $\beta_1$	0.9
Adam/VRAdam $\beta_2$	0.999
Adam/VRAdam $\epsilon$	$1 \times 10^{-8}$
VRAdam power	2
SGD momentum	0.2
SGD nesterov	True
RMSProp alpha	0.1
RMSProp $\epsilon$	$1 \times 10^{-8}$
RMSProp momentum	0.2

Table 12: Swept Hyperparameters during Diffusion Comprehensive Sweep

Optimizer	Parameter	Sweep Configuration	Optimal Parameter
VRAdam	$\eta$	Log-uniform, Min: $1 \times 10^{-5}$ , Max: $1 \times 10^{-1}$	$3.38 \times 10^{-5}$
VRAdam	$\beta_3$	Uniform, Min: 0.1, Max: 2.0	1.99
VRAdam	lr cutoff	Integer Uniform, Min: 5, Max: 30	6
VRAdam	normgrad	Values: [True, False]	True
Adam	$\eta$	Log-uniform, Min: $1 \times 10^{-5}$ , Max: $1 \times 10^{-1}$	$3.24 \times 10^{-5}$
SGD	$\eta$	Log-uniform, Min: $1 \times 10^{-5}$ , Max: $1 \times 10^{-1}$	0.00227
RMSProp	$\eta$	Log-uniform, Min: $1 \times 10^{-5}$ , Max: $1 \times 10^{-1}$	$1.81 \times 10^{-5}$

Method	Validation Loss	Test Loss
VRAdam	0.0360	0.0360
AdamW	<b>0.0354</b>	0.0354
SGD+Nesterov	0.056	0.054
RMSProp	0.0363	<b>0.0350</b>

Table 13: Diffusion model results on MNIST.

## B.5 Edge of Stability analysis

Table 15: Hyperparameters edge of stability analysis

Parameter	Value
Model Architecture	ResNet 32
Max iterations	20000
Batch Size	1000
Seed	0
Loss criterion	Mean squared error
VRAdam $\eta$	0.002
VRAdam $\beta_1$	0.9
VRAdam $\beta_2$	0.999
VRAdam $\beta_3$	1
VRAdam power	2
VRAdam normgrad	False
VRAdam lr cutoff	19
VRAdam $\epsilon$	$1 \times 10^{-7}$
Adam $\beta_1$	0.9
Adam $\beta_2$	0.999
Adam $\epsilon$	$1 \times 10^{-7}$

## C Compute Resources

All experiments were run on Lambda cloud instances or the Google cloud platform (GCP). Experiments were conducted either using a NVIDIA L4 GPU with 24 GB of GPU memory and 31 GB of system memory or larger experiments were performed on a NVIDIA A10 with 24 GB of GPU memory and 200 GB of system memory.

## D Loss curves with Error Envelopes

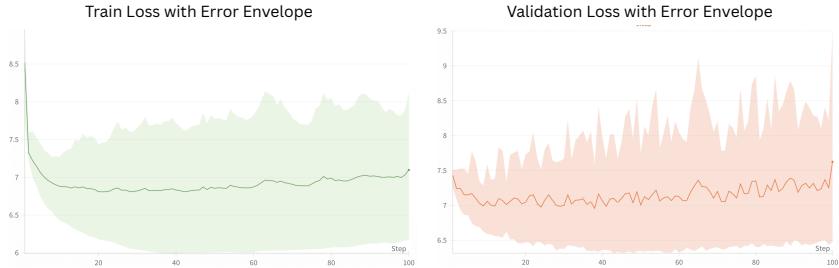


Figure 4: Train (left) and validation (right) loss curves with error envelopes calculated using different run values for language modeling using AdamW.

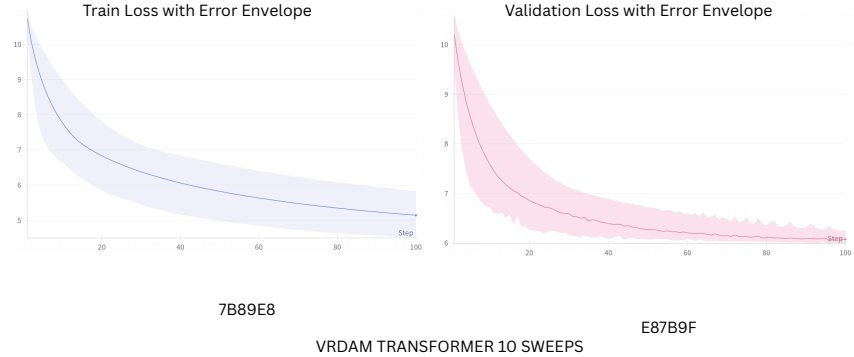


Figure 5: Train (left) and validation (right) loss curves with error envelopes calculated using different run values for language modeling using VRAdam.

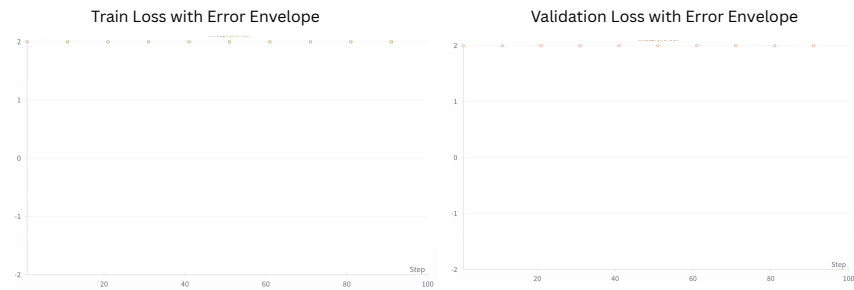


Figure 6: Train (left) and validation (right) loss curves calculated using different run values for language modeling using SGD Nesterov with momentum. The dots on the top indicate NaN values.

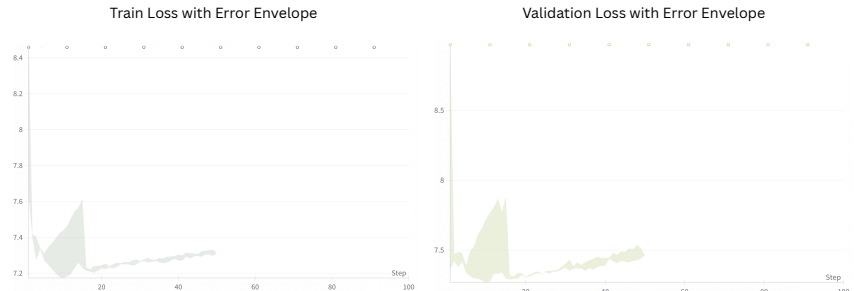


Figure 7: Train (left) and validation (right) loss curves with error envelopes calculated using different run values for language modeling using RMSProp. The dots on the top indicate NaN values.



Figure 8: Train (right) curves with error envelopes calculated using different run values for image classification using VRAdam. Test loss values (left) over different runs.

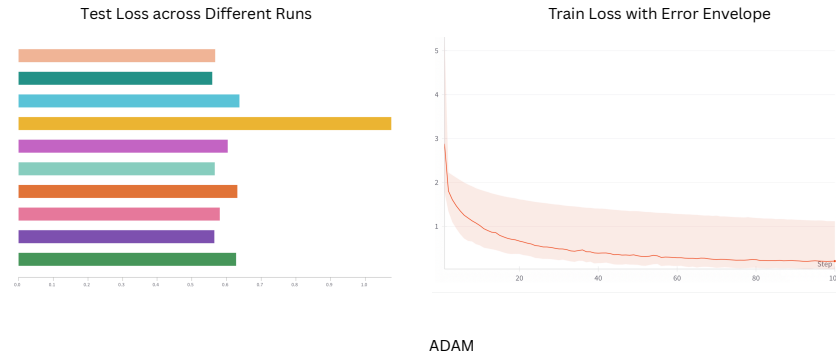


Figure 9: Train (right) curves with error envelopes calculated using different run values for image classification using AdamW. Test loss values (left) over different runs.

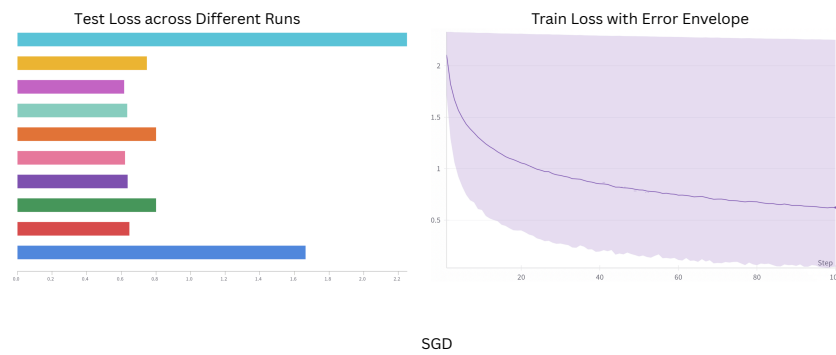


Figure 10: Train (right) curves with error envelopes calculated using different run values for image classification using SGD Nesterov with Momentum. Test loss values (left) over different runs.

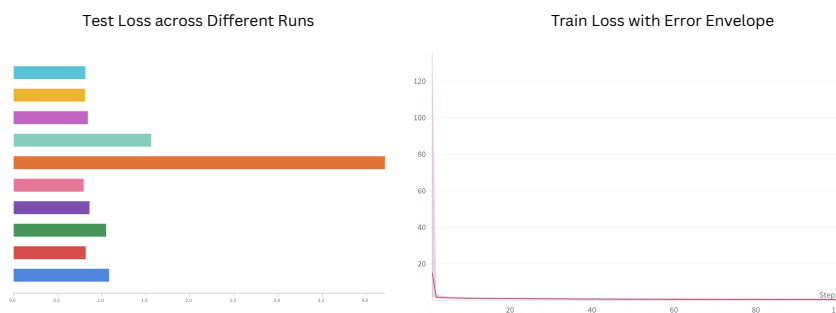
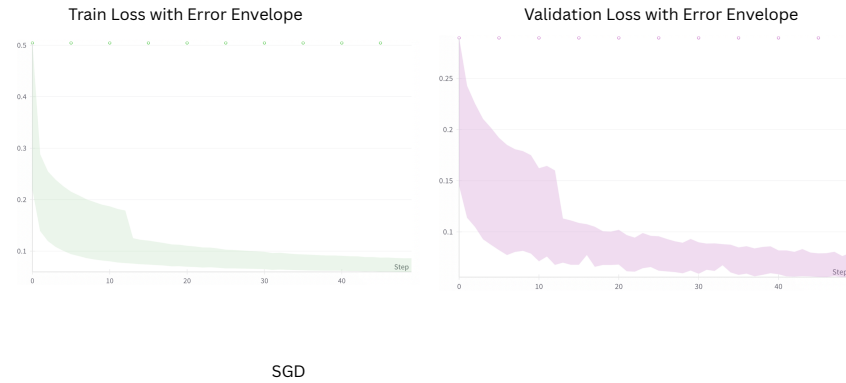


Figure 11: Train (right) curves with error envelopes calculated using different run values for image classification using RMSProp. Test loss values (left) over different runs.



SGD

Figure 12: Train (left) and validation (right) loss curves calculated using different run values for the diffusion model using SGD Nesterov with momentum.

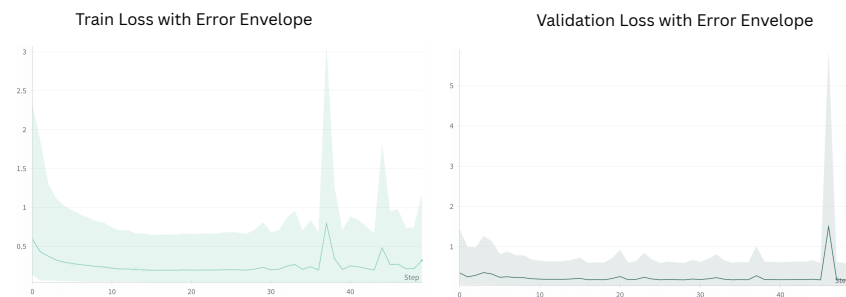


Figure 13: Train (left) and validation (right) loss curves calculated using different run values for the diffusion model using RMSProp.